Chapter 1

Detectors for digital mammography

Andrew Karellas and Srinivasan Vedantham

Introduction

Mammography is the most technically demanding radiographic modality, requiring high spatial resolution, excellent low contrast discrimination, and wide dynamic range. The development of dedicated mammography systems [1] in the mid-1960s and the refinements in film-screen technology over its long evolution [2,3] were of critical importance in establishing the benefits of mammography in reducing breast cancer mortality [4–10]. The use of film-screen technology over 30 years ensured excellent spatial resolution under optimal conditions. The high spatial resolution requirement was thought to be essential for imaging small and subtle calcifications as small as 100–200 μm, in particular for visualizing its morphology. In spite of the excellent imaging characteristics of film-screen technology under optimal exposure and film development conditions, intrinsically images are more susceptible to artifacts. Small deviations from optimal exposure and processing conditions can have profound effects on mammographic image quality, such as its ability to provide a balanced image over regions of the breast that vary in radiographic density. The well-documented weaknesses of film-screen technology [11–13] include limited dynamic range, limited tolerance to exposure conditions, complexity and instabilities due to the chemical processing of film, and the lack of ability to digitally communicate, store, and enhance the images.

Digital mammography, a term coined for electronic image capture of x-rays transmitted through the breast, is a concept that was formed about 30 years ago as a means of circumventing some of the major limitations of film-screen technology. An electronic imaging detector that replaces film-screen for image capture would minimize the possibility of suboptimally exposed mammograms, which can potentially conceal subtle soft tissue lesions and microcalcifications. Digital mammography can provide wide dynamic range, wide exposure latitude, and the ability to communicate, store, and digitally manipulate images. The concept of computer-aided detection and diagnosis (CADe and CADx) [14,15] was envisioned even before digital mammography became a reality, and the idea of obtaining mammograms using electronic image capture was certainly very attractive as an enabling technology for further development and proliferation of computer-aided techniques. Convenient digital storage and communication of mammographic images was another potential advantage that fueled the early development of digital mammography. The ensemble of all these positive attributes served as the overall motivation for seeking replacement of film-screen with digital mammography, in the belief that the benefits provided by digital mammography would improve detection, diagnosis, and management of breast cancer.

In the early days of investigations into the potential of digital mammography, particularly those pertaining to digital communication, image enhancement, and computer-aided techniques, digitization of film mammograms was used as a proxy because of the unavailability of digital mammography detectors. Digitization was accomplished by flying spot scanners, video cameras, and eventually high-resolution digital scanners. This early experience with digitized mammograms was important, because it provided an early experience of digital enhancement techniques, understanding the need for digital communication and storage, and most importantly it acted as a platform for the development and evaluation of CADe/CADx. Creation of databases with digitized mammograms for teaching and research that were readily accessible through the internet [16] was also particularly important in improving our understanding of image display (monitor) requirements and the tools needed by the user for digital image manipulation. Several studies demonstrated techniques for enhancing digitized mammograms, and others reported on the "equivalence" of digitized mammograms to the original film mammograms. Digitized mammograms added another dimension to film-screen mammography, and considering some of the initial challenges in the development of digital mammography detectors, it appeared that replacing film-screen mammography was a nearly impossible task.

One of the beliefs during the developmental stages of digital mammography was that the detectors designed for digital mammography should replicate many of the desirable characteristics of film-screen technology while circumventing

Digital Mammography: A Practical Approach, ed. Gary J. Whitman and Tamara Miner Haygood. Published by Cambridge University Press.

all of its limitations. This assumption made it particularly challenging during the development of digital mammography detectors, considering that film-screen technology had undergone many improvements such as development of screens and film with increased sensitivity and refinements in chemical processing. The development of digital detectors to cover the entire breast, and with spatial resolution comparable to film-screen technology, required digital detectors with an effective pixel size of 20 μm or less. Attaining this spatial resolution seemed impossible then, and it is still unrealistic even with current technology. The theoretical basis of the complex interplay between resolution, image noise, and radiation dose was well known [17–19]. The construction and characterization of early prototypes of digital mammography detectors allowed comparison of their physical imaging properties with film-screen technology, in particular understanding the trade-off between spatial resolution and image noise that was essential in mitigating some of the concerns about the pixel size used by digital mammography detectors.

The term digital mammography is generally used for any technology that performs electronic image capture of x-rays transmitted through the breast. However, the technological implementations of digital mammography utilize various principles for image formation that also affect the resultant image quality. This necessitates a discussion of the image quality metrics used to describe the performance of digital mammography systems.

Image quality metrics

Mammography systems must possess certain desired characteristics in terms of spatial resolution, image noise transfer, dynamic range, fixed pattern noise, artifacts, and dose efficiency. Several universally accepted metrics have been developed that can be used for the evaluation of the performance of digital mammography systems. These metrics can be either observer-independent or observer-dependent. The observer-independent metrics may be based on analysis in the spatial or image domain or in the spatial frequency domain. These metrics are summarized in Table 1.1. If one considers a continuous spatial distribution of x-rays on the detector surface, then the resultant signal is sampled by the pixels which are spatially separated by the pixel pitch, represented as Δ. Then, the cut-off spatial frequency (ω_c) is defined as $\omega_c = 1/\Delta$, and the spatial frequency above which aliasing (degradation due to undersampling) occurs is defined by the Nyquist frequency $\omega_N = 1/2\Delta$. In terms of spatial resolution, three of the metrics are related: resolution in the spatial domain, typically represented by the point spread function (PSF) or the related spread functions such as the line spread function (LSF) and the edge spread function (ESF); the observer-dependent limiting resolution, which is the smallest spacing between "line-pairs" or the highest line-pairs/mm the observer is able to visualize; and the modulation transfer function (MTF) in the spatial frequency domain. The modulation transfer function is a measure of the signal transfer property of the imaging system and provides the factor by which the output signal amplitude is reduced compared to the sinusoidal input at different spatial frequencies. The spatial domain objective metric LSF is related to the spatial frequency domain MTF by the modulus of its Fourier transform normalized to a peak of unity at zero spatial frequency. MTF is a dimensionless quantity. Figure 1.1 shows an example, where system A has a narrower point spread function (reduced blur) than system B. The corresponding MTF shown on the right indicates that system A has improved MTF compared to system B. The concept of presampling MTF is used with digital imaging systems so as to minimize the phase/sampling effects that can affect the measurements [20–22].

Table 1.1 Observer-dependent and observer-independent image quality metrics that are used to assess digital mammography system performance.

Image quality metrics	
Objective (observer-independent)	**Perceptual (observer-dependent)**
Spatial domain metrics	
Resolution (PSF)	Limiting resolution
Noise (standard deviation, variance)	Threshold contrast-detail
Contrast (signal difference to noise ratio)	Alternative forced choice (AFC)
	Receiver operating characteristics (ROC)
Spatial frequency domain metrics	
Modulaton transfer function	
Noise power spectrum	
Noise equivalent quanta	
Detective quantum efficiency	

The observer-dependent limiting resolution is typically the spatial frequency at which the MTF is approximately in the range of 0.05–0.1, provided the detector sampling (pixel pitch) does not result in aliasing. As an example, let us assume systems A and B shown in Figure 1.1 have pixel pitch of 100 μm and the x-ray source focal spot is too small to have an effect. The Nyquist spatial frequency for both systems is 5 cycles/mm [=1/(2×0.1-mm)] and the cut-off frequency is 10 cycles/mm [=1/(0.1-mm)]. The spatial frequency at which the MTF is 0.1 is approximately 3 and 6 cycles/mm for systems B and A, respectively. Let us assume that a high-contrast line-pair test object, such as that shown in Figure 1.2, is imaged after positioning on the detector surface so that there is negligible magnification and it is aligned with the pixel orientation. For system B, an observer would be able to perceive approximately 3 line-pairs/mm, corresponding to the spatial frequency at which the MTF is 0.1, as it is lower than the Nyquist frequency. For system A, the limiting resolution that the observer perceives without aliasing effects would be approximately 5 line-pairs/mm, corresponding to the Nyquist frequency, even though the spatial frequency at which MTF is 0.1 is 6 cycles/mm. However, if the test object is moved closer to

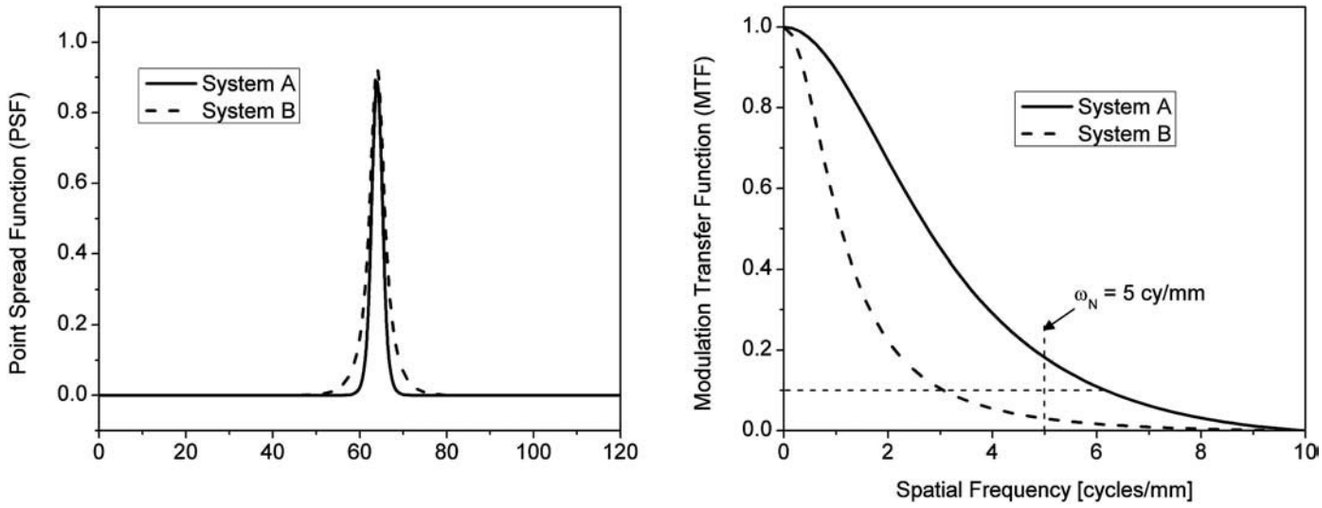

Figure 1.1 Relationship between point spread function (PSF) and modulation transfer function (MTF). System A has a narrower PSF, resulting in a higher MTF, compared to system B.

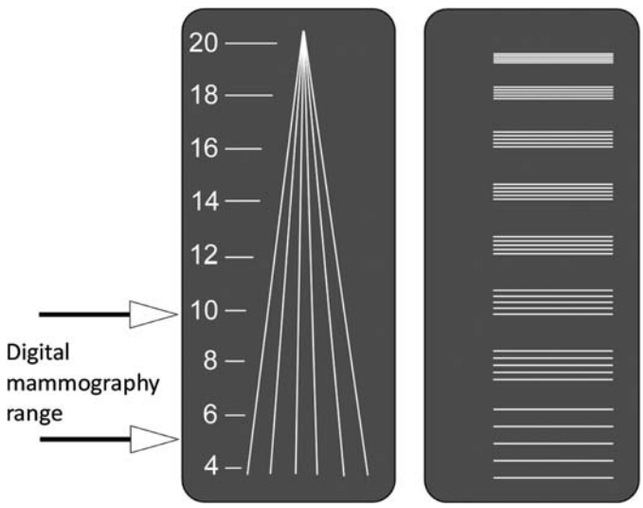

Figure 1.2 Examples of resolution test patterns used for assessing perceived limiting resolution (not to scale).

the source, resulting in magnification (for example 1.8 times, as typically used in magnification mammography), and assuming the x-ray focal spot size does not contribute to blur, then it would be possible to perceive a limiting resolution of 6 line-pairs/mm with system A. Thus under conditions of negligible magnification, the limiting resolution that is perceived using a line-pair test object without aliasing effects is the minimum of the Nyquist spatial frequency or the spatial frequency at which the modulation transfer function has a value of approximately 0.1. Perceived limiting resolution with a test pattern is often used for monitoring system image quality, and is performed as part of annual quality control procedures for mammography systems.

The noise power spectrum (NPS) provides the spatial frequency domain representation of the image noise, and the integral of the NPS is identical to the second-order spatial domain noise metric, the variance. This implies that for Poisson-distributed incident x-ray quanta at a given exposure or air kerma, measurement of the NPS can provide the noise transfer properties of the system at that exposure. NPS is determined by ensemble average of the squares of the magnitude of Fourier-transformed images or regions of interest acquired with uniform exposure to the detector. If the acquired images are represented in digital units (DU), then the NPS has units of $DU^2.mm^2$. Alternatively, if the images are transformed from DU to electrons, exposure (mR), or air kerma (mGy), then the units for NPS are correspondingly altered. It is important to note that the measured NPS includes aliasing effects and hence the NPS is only defined up to the Nyquist sampling limit. Often the term "normalized NPS" is also used to represent the image noise at a given exposure, which represents the measured NPS divided by the square of the mean large-area signal at that exposure. If one considers an x-ray spectrum with x-ray photon fluence per unit (mR) exposure of q_0/X photons/(mm^2.mR) and exposure incident on the detector of X_i mR, then the photon fluence is $(q_0/X)X_i$ photons/mm^2. The large-area mean signal at uniform exposure to the detector, X_i, can be represented as S_i. Then the normalized NPS is represented as $\hat{W}(u, v) = W(u, v)/S_i^2$, where $W(u, v)$ is the NPS measured at the exposure X_i. Typically, the signal S_i increases with increase in exposure X_i either in a linear fashion or in a predefined manner such as logarithmic or square-root response, depending on the detector readout technology. The NPS, $W(u, v)$ will also exhibit a similar response with increasing exposure provided the additive system noise is not dominant. Hence, the normalized NPS, $\hat{W}(u, v)$ will exhibit decreased amplitude when exposure X_i is increased. Thus, the exposure dependency will be reversed between the NPS and the normalized NPS. In addition, normalization by S_i, which is represented in DU, would also result in change of units for the normalized NPS to mm^2.

Noise equivalent quanta (NEQ) is an important metric derived from the large-area mean signal, MTF, and NPS and represents the square of the signal-to-noise ratio at a given exposure to the detector. It is computed as $NEQ(u,v) = S_i^2 MTF^2(u,v)/W(u,v)$, or equivalently as $NEQ(u,v) = MTF^2(u,v)/\bar{W}(u,v)$. From the above mathematical description, it is apparent that NEQ has units of mm^{-2}, as MTF is dimensionless and the normalized NPS has units of mm^2. NEQ facilitates task-specific system optimization [23] such as selecting the appropriate applied tube voltage (kVp) and x-ray beam filtration so as to maximize the signal-to-noise ratio. It also facilitates comparison across multiple detector technologies. Another important derived metric is the detective quantum efficiency (DQE), which provides the signal-to-noise ratio transfer characteristics of the system and is a measure of dose efficiency. It is computed as,

$$DQE(u,v) = \frac{S_i^2 MTF^2(u,v)}{[(q_0/X)X_i]W(u,v)} = \frac{NEQ(u,v)}{[(q_0/X)X_i]}.$$

Since, NEQ has units of mm^{-2} and the photon fluence $(q_0/X)X_i$ also has units of mm^{-2}, DQE is a dimensionless quantity. For Poisson-distributed x-ray quanta, where the mean is equal to its variance, the term $(q_0/X)X_i$ represents the variance of the x-ray beam incident on the detector at the exposure X_i. Thus, DQE represents the ratio of the square of the signal-to-noise ratio at image output to that at detector input, providing the signal-to-noise ratio transfer characteristics of the system. Also, for a defined x-ray beam quality (kVp, filtration), the term $(q_0/X)X_i$ is proportional to the radiation dose, and hence DQE can also provide a measure of dose efficiency.

The spatial domain metric contrast provides the difference in signal values between two locations that differ in x-ray attenuation properties. However, with digital imaging systems that allow easy manipulation of image data values, contrast is usually computed as the signal difference to noise ratio (SDNR). It is computed as $SDNR = |S_b - S_o|/\sigma_b$, where S_b and S_o represent the mean signal values of the background and the signal object, and σ_b represents the standard deviation of the background. Alternative descriptions for the standard deviation such as $\sqrt{\sigma_b^2 + \sigma_o^2}$, which takes into account the standard deviation of the signal intensities within the object, may also be used in SDNR computation. Contrast measurements with test phantoms, such as the American College of Radiology (ACR)-recommended accreditation phantom, are often used for monitoring system image quality and are performed as part of annual quality control procedures for mammography systems [24].

All of the image quality metrics described above, with the exception of the perceived limiting resolution, do not involve the observer. Threshold contrast-detail measurements provide a powerful tool that takes into account the signal object size, its contrast, and the image noise as perceived by the observer. A typical contrast-detail phantom contains a homogeneous background with circular disk-shaped signal objects that are arranged in a square matrix and vary in diameter along one direction that provides changes in object size, and in disk thickness along the orthogonal direction that provides changes in image contrast. The observer or group of observers determines for each row and column the signal objects that are visualized. For each disk diameter (detail size), the disk thickness (contrast) that is just visualized by the observer or group of observers is plotted to generate the contrast-detail diagram, which provides the threshold contrast-detail characteristics of the system. One major limitation of this approach is that the ordered matrix of signal objects allows observers to predict the location of objects that may be difficult to visualize without this prior knowledge.

Alternative forced choice (AFC) methodology can overcome this limitation. In this approach the signal object may be located in one of multiple locations, and the observer has to indicate its location even if the signal object is difficult to visualize because of its size, contrast, or the noise present in the images. Since the observer is "forced" to choose the location of the signal from multiple locations (alternative choice), the term "alternative forced choice" is used. Additionally, the methodology allows estimating contrast-detail characteristics at different threshold levels. Figure 1.3 shows an example of a phantom that is designed for conducting AFC studies in mammography [25]. This phantom has a homogeneous background with a matrix of cells that contain circular disk-shaped signal objects, which vary in diameter along one direction and in thickness along the orthogonal direction. Each cell has two signal objects, one at its center and the other at one of its four corners. For the AFC study, the signal object located at the center of a cell is ignored and the observer has to select one of the four corners, i.e., four alternative choices, in which the signal object is perceived. The probability that an observer may randomly pick the correct corner is 1/4 (0.25). Thus the fraction of correct responses, often referred to as percent correct detection, will range from 0.25 to 1.0. Figure 1.4 shows an example of percent correct detection for three disk diameters based on image interpretation by one observer of hard-copy digital images of the phantom [25]. The 50% threshold level is shown by the horizontal line and its intercept with the curves for the three disk diameters projected to the x-axis (disk depth that provides a measure of contrast) is used to generate the contrast-detail diagram. Figure 1.5 shows an example of contrast-detail characteristics obtained at 62.5% threshold for a film-screen mammography system and hard-copy images from a digital mammography clinical prototype system [25]. It is important to note that these are *threshold* contrast-detail characteristics, and thus a system exhibiting improved contrast-detail characteristics would be represented by a curve lower than the other. An ideal system would exhibit threshold contrast-detail characteristics that follow the axes, i.e., even a small signal object (detail size) is visualized with high contrast. While the specific phantom described above has a homogeneous background, AFC methodology can also be used for studies with heterogeneous backgrounds such as

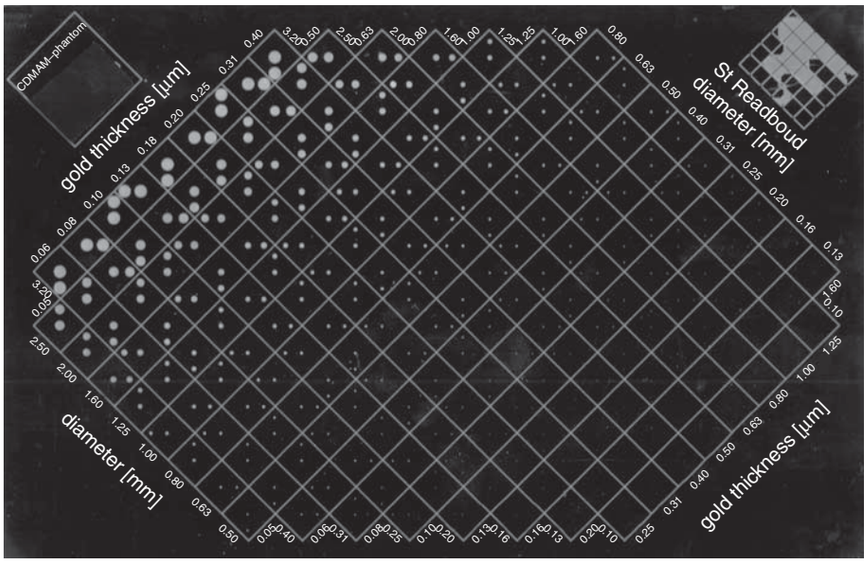

Figure 1.3 CDMAM phantom that can be used for AFC studies of mammography systems. Reproduced with permission from Suryanarayanan *et al.*, *Radiology* 2002; **225**: 801–7 [25]. © Radiological Society of North America.

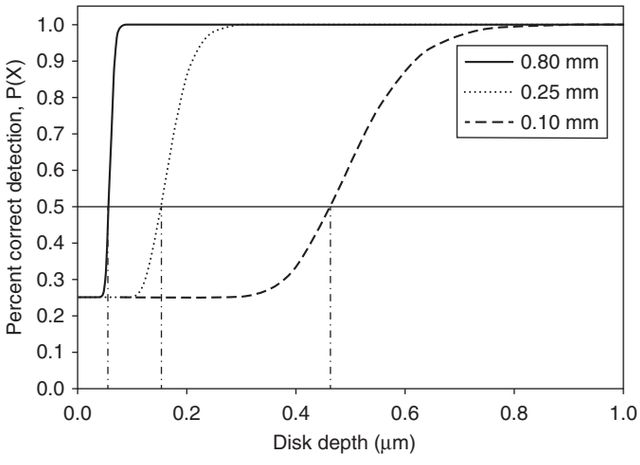

Figure 1.4 Percent correct detection for three disk diameters used for computing threshold contrast-detail characteristics using AFC methodology. Reproduced with permission from Suryanarayanan *et al.*, *Radiology* 2002; **225**: 801–7 [25]. © Radiological Society of North America.

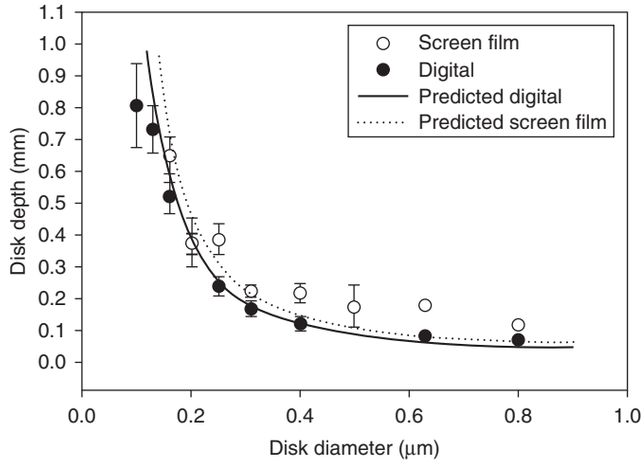

Figure 1.5 Contrast-detail characteristics obtained at 62.5% threshold using AFC methodology. Reproduced with permission from Suryanarayanan *et al.*, *Radiology* 2002; **225**: 801–7 [25]. © Radiological Society of North America.

the anatomical background due to overlapping tissue structures encountered in mammography [26].

The standard and best-established perceptual image quality metric that is of direct clinical relevance is the receiver operating characteristic (ROC), which provides sensitivity/specificity characteristics. Considering the extensive use of ROC methodology in medical imaging, and the availability of excellent texts on this topic [27,28], only a brief description is provided. ROC methodology not only allows comparison across different technologies within the same modality, e.g., film-screen versus digital mammography, it also allows comparison across different modalities, e.g., mammography versus breast ultrasound. The methodology is suitable not only for detection tasks based on observer's confidence in the presence of a lesion in an image, but also characterization tasks based on observer's confidence that the lesion present is malignant. In a typical ROC study, an observer provides a rating based on a predefined scale for the intended task and this rating is analyzed with knowledge of "truth." Software programs to fit observer ratings to an ROC curve and calculate the statistical significance of differences between ROC index estimates and parameters are available [29].

Description of the image quality metrics and understanding their importance is necessary to contrast the different digital mammography detector technologies that are currently used in practice. Broadly, it is convenient to classify the

detector technologies into indirect and direct conversion, based on the physical principle used for image formation.

Indirect conversion with prompt readout

The indirect-conversion approach with prompt readout of the signal is similar to the basic principle used in film-screen technology. This process uses a scintillator, typically a thin layer of thallium-doped cesium iodide or gadolinium oxysulfide. X-rays transmitted though the breast pass though the breast support plate and the antiscatter grid, and interact with the scintillator primarily by the photoelectric effect. In response to the x-ray interaction the scintillator emits light predominantly in the green region of the electromagnetic spectrum and proportional to the energy of the interacting x-ray photon that is detected by an optically sensitive detector (photodetector). This seemingly simple approach had been technologically difficult to accomplish until the last decade. Technological implementation of the indirect conversion with prompt readout varies based on the scintillator and the photodetector used.

Scintillator

The physical characteristics of the scintillator are critical for attaining good spatial resolution and contrast at a low radiation dose. Gadolinium oxysulfide polycrystalline granular scintillators, which have been used widely as intensifying screens in film cassettes, were initially used with small-field-of-view digital mammography systems [30] and early full-field digital mammography system designs [31], largely because of the unavailability of alternatives. However, they were not well suited as scintillators in digital mammography. A major reason is the difference in the geometry of x-ray projection between film-screen and digital mammography. As depicted in Figure 1.6 (right), x-rays must first pass though the film to reach the screen, and this is done by design in order to minimize light diffusion in the screen and thereby preserve spatial resolution. This geometry ensures that scintillations generated from each x-ray photon interaction within the screen predominantly occur close to the film surface because of exponential x-ray attenuation. In digital mammography, this geometry is not replicated (Figure 1.6, left) and it is challenging to implement because x-rays must first penetrate the detector substrate and photodetector before the scintillator. The detector substrate, depending on the optically sensitive detector and the readout technology, is typically a glass plate with a thickness of about 1 mm, which could cause partial x-ray attenuation. Therefore, with available detectors, the scintillators must be placed such that the x-ray beam interacts with the scintillator before the photodetector. In this configuration a higher fraction of x-ray interactions in the scintillator occur further from the photodetector, and the larger path length of the scintillations before reaching the photodetector contributes to increased light diffusion, which degrades spatial resolution. While reducing the scintillator layer thickness could reduce the path length and consequently improve spatial resolution, this results in reduced x-ray stopping power or quantum efficiency. Therefore, scintillators for digital mammography must possess certain characteristics that ensure high quantum efficiency with minimal degradation of the resolution.

Out of hundreds of known scintillators, currently only one, thallium-doped cesium iodide (CsI:Tl) has been deemed suitable for digital mammography. This scintillator can be vapor-deposited on a number of substrates or directly on the optically sensitive detector. Direct deposition of the scintillator on the detector is desirable for efficient light transmission that will deliver adequate signal to the silicon photodetector. The vapor deposition is important, as it forms a needle-like structure that reduces lateral diffusion of the scintillations caused by x-ray interaction by predominantly channeling the light through the process of internal reflection, in essence acting like pseudo-fiberoptics. This structure is shown in the scanning electron microscope image in Figure 1.7. The pseudo-fiberoptic structure allows the use of a thicker scintillator layer to improve quantum efficiency, with minimal degradation in spatial resolution. On average, each interacting 1 keV x-ray photon generates approximately 50–55 optical photons. This scintillator has good transparency to the scintillations generated, i.e., reduced self-attenuation of optical photons, that transports most of the scintillations to the photodetector. In addition, the wavelength of emission is well matched to the absorption characteristics of silicon-based photodetectors, resulting in good efficiency. Typically, digital mammography systems use a layer of CsI:Tl 100–150 μm thick, and the quantum efficiency as a function of incident x-ray photon energy is shown for the energy range of 5–40 keV in Figure 1.8. A nominal value for packing fraction, which defines the volume occupied by the phosphor

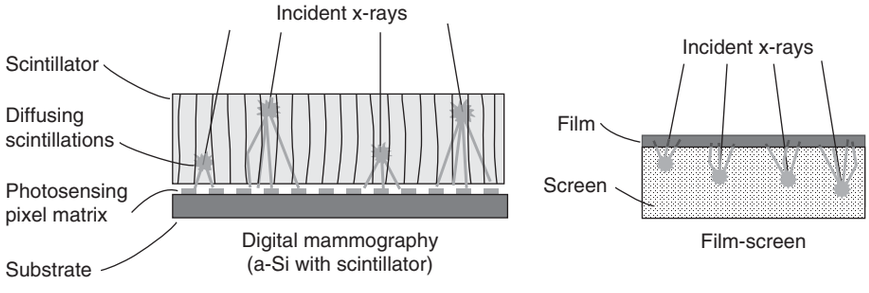

Figure 1.6 Comparison of imaging geometry used with film-screen mammography and digital mammography based on indirect conversion with prompt readout.

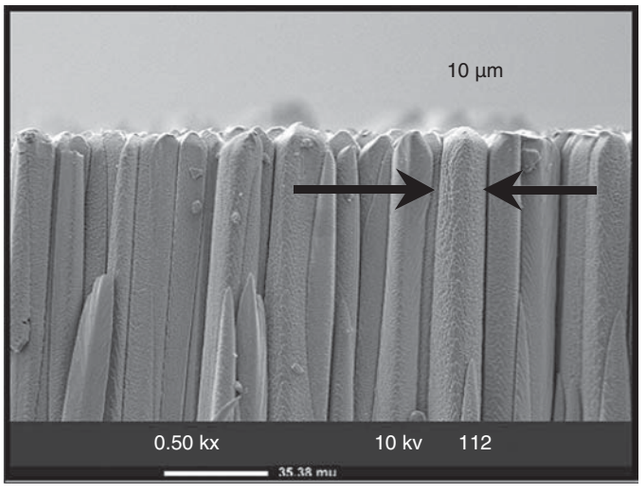

Figure 1.7 Scanning electron microscope image of a CsI:Tl scintillator, showing the needle-like structures. Courtesy of Vivek Nagarkar, PhD, RMD Inc., Watertown, MA.

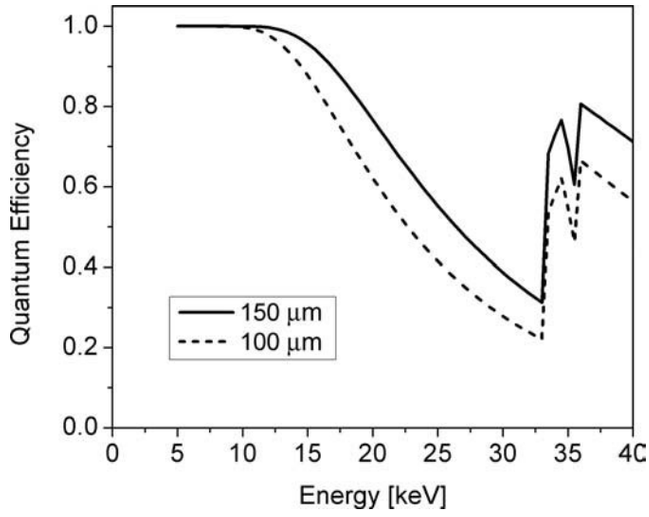

Figure 1.8 Quantum efficiency of CsI:Tl 100 and 150 µm thick, with 80% packing fraction in the energy range 5–40 keV.

grains within this layer, of 80% was assumed for these calculations. The integration of CsI:Tl with the photodetector presented several challenges in manufacturing, particularly in the direct deposition onto the photodetector array and protection from humidity, because of the hygroscopic nature of CsI:Tl. These early challenges have been overcome, and integrated digital mammographic detector assemblies of this type are now produced routinely by at least one major manufacturer.

Photodetector

Currently, the most commonly used photodetector technology is the flat-panel amorphous silicon photodiode array with thin-film transistor readout. Although scintillator development for mammography presented some challenges for the industry in terms of optimizing CsI:Tl thickness, optimizing thallium dopant concentration, which can affect light output, and refining direct deposition techniques, the properties of CsI have been known for many years. However, pixilated amorphous silicon detectors are a relatively new technology, and the first commercially intended devices were manufactured only in the mid-1990s. The detector consists of a thin layer of amorphous silicon (a-Si) with a thickness of a few µm that is deposited on a glass substrate with a thickness of about 1 mm (Figure 1.6, left). The photodetector consists of an array of approximately 2400 × 3000 photosensitive elements (pixels) for a 24 × 30 cm detector. The detector consists of the hydrogenated amorphous silicon (a-Si:H) photodiode, the photosensitive part of the detector that responds to the optical signal from the scintillator, the a-Si:H thin-film transistor, and the bias, gate, and data channels. The a-Si layer is the light-sensitive part of the flat-panel plate with a quantum efficiency of about 50–65% for the light emitted by a CsI:Tl scintillator. The bias channels supply the voltage, and the gate channels control the signal readout of the panel. It is important to note that the signal-detecting a-Si photodiode occupies only a fraction of the pixel area on the a-Si flat-panel detector with the remainder taken up by other structures such as the bias, gate, and data lines and the thin-film transistor. The size of each a-Si detector element is about 100 µm. Geometrical fill factor, defined as the ratio of the area occupied by the optically sensitive region (a-Si photodiode) to the pixel area, can vary with different flat-panel detector designs, but with current technology achieving approximately 75% fill factor is considered high. Higher fill factors approaching unity are desirable so as to maximize the capture of the optical signal from the scintillator. It is relevant to note that the CsI:Tl scintillator layer is deposited as a continuous layer covering the entire detector, and only the a-Si photodiode array with thin-film transistor readout is a discrete array.

The a-Si with scintillator (indirect-conversion) approach was the first large-scale attempt for full-breast digital mammography, also known as full-field digital mammography (FFDM). Initially, a-Si flat-panel detectors did not appear suitable for digital mammography. Early results with a-Si with a scintillator for x-ray imaging applications seemed promising, but their adaptation to mammography seemed a distant goal because of the electronic noise levels and the relatively large 100 µm detector elements. The resulting limiting resolution of 5 line-pairs/mm, compared to about 18 line-pairs/mm for film-screen mammography, was also perceived as a severe limitation. Despite these concerns, clinical performance [32,33], physical [34,35], and perceptual [25] evaluations have demonstrated important advantages over film-screen mammography. Figure 1.9 shows the objective physical performance metric, DQE, measured for a clinical FFDM system at 28 kVp with a molybdenum anode, rhodium-filtered (Mo/Rh) x-ray spectrum after transmitting through 45 mm of polymethyl methacrylate (PMMA) [34]. Continuing evolution of this detector technology [36], in part to address the needs of breast imaging techniques such as digital breast tomosynthesis and contrast-enhanced digital mammography, can be observed with

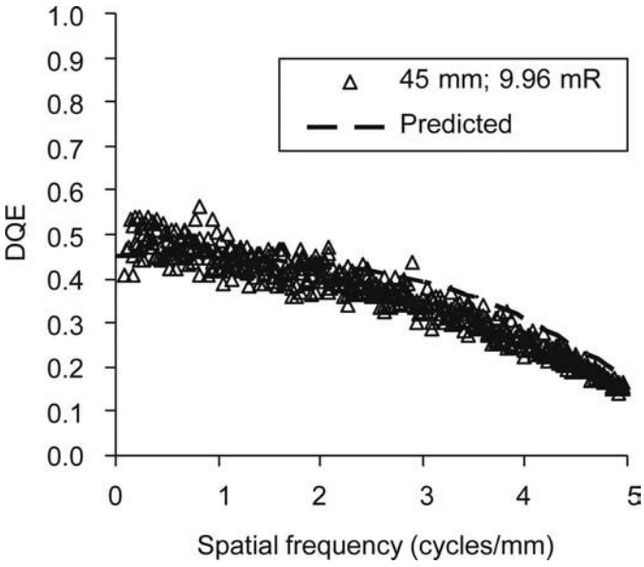

Figure 1.9 DQE measurements performed on an amorphous silicon (a-Si)-based full-field digital mammography (FFDM) system at 28 kVp Mo/Rh x-ray spectrum filtered with 45 mm of PMMA. Reproduced with permission from Suryanarayanan *et al.*, *Nucl Instrum Methods Phys Res A*, 2004; **533**: 560–70 [34]. © Elsevier B.V.

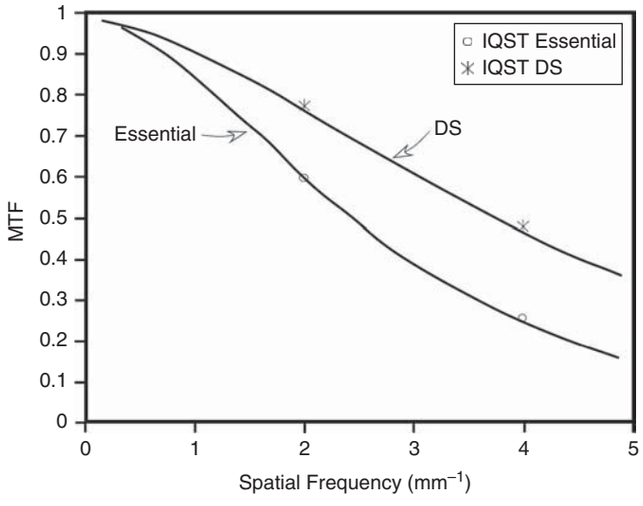

Figure 1.10 MTF measurements performed on two versions of amorphous silicon (a-Si)-based FFDM systems. Adapted with permission from Ghetti *et al.*, *Med Phys* 2008; **35**: 456–63 [36]. © American Association of Physicists in Medicine.

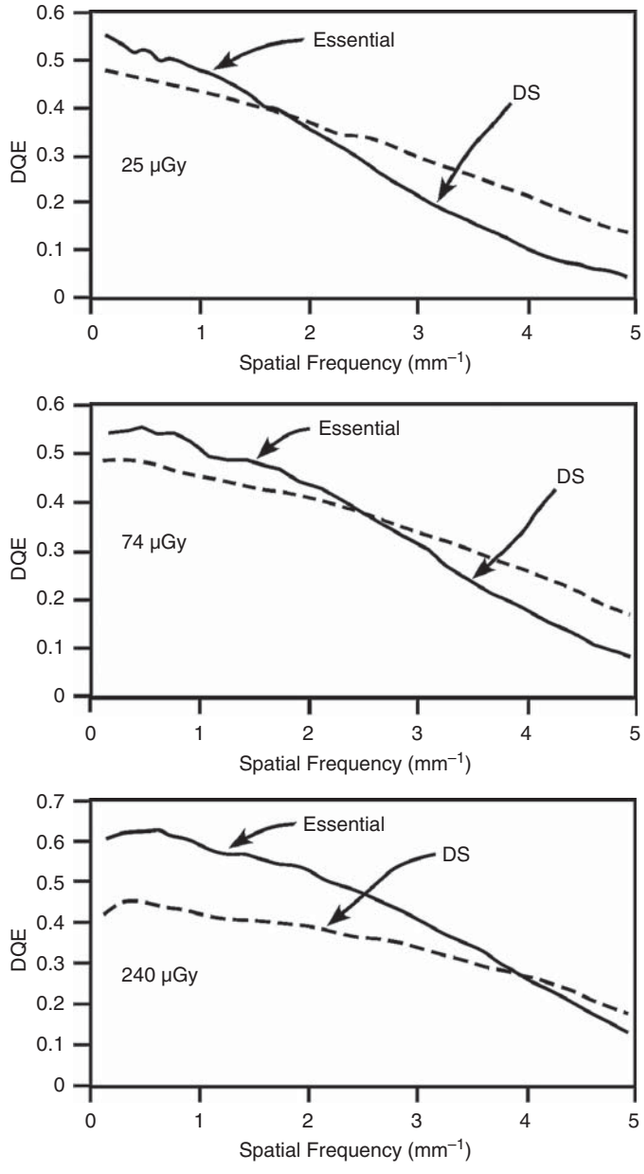

Figure 1.11 DQE measurements performed on two versions of amorphous silicon (a-Si)-based FFDM systems. Adapted with permission from Ghetti *et al.*, *Med Phys* 2008; **35**: 456–63 [36]. © American Association of Physicists in Medicine.

changes in MTF and DQE shown in Figures 1.10 and 1.11, respectively. Thus, current versions of CsI:Tl coupled a-Si-based indirect-conversion detectors provide a low-frequency DQE, in the range of 0.5–0.6 for exposure levels relevant to mammography.

Alternative photodetector technologies such as charge-coupled devices (CCDs) and complementary metal-oxide semiconductors (CMOS) are also of interest in the indirect-conversion approach with prompt readout. Small-field-of-view digital mammography systems [30] used for spot compression views and stereotactic locations, as well as early generations of FFDM systems [31,37], used charge-coupled devices for readout. CMOS technology, in particular systems employing on-pixel amplification to increase signal intensity relative to noise, is being actively researched as a possible candidate for digital mammography [38,39].

Direct conversion

The direct-conversion approach eliminates the scintillator, and a photoconductive amorphous selenium (a-Se) layer with a thickness of about 200–250 μm is used as the primary detector

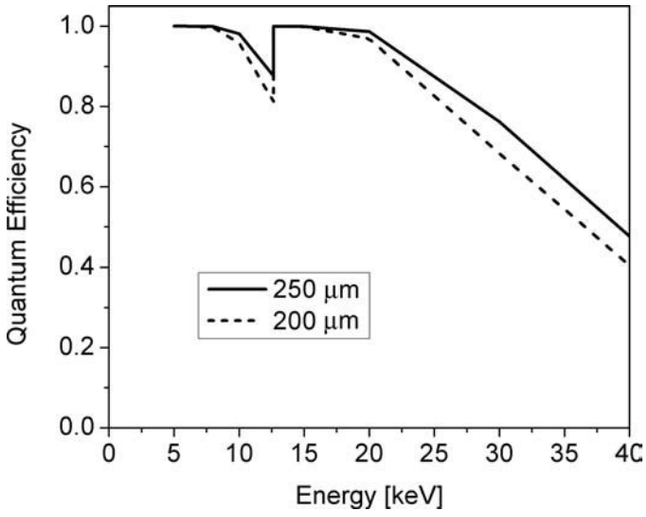

Figure 1.12 Quantum efficiency of a-Se layers 200 and 250 µm thick with 80% packing fraction.

of x-rays. Figure 1.12 shows the computed quantum efficiency for a-Se layers 200 and 250 µm thick as a function of incident x-ray photon energy in the range of 5–40 keV. X-rays are transmitted past the breast, traverse through a thin continuous electrode layer, and interact in the a-Se layer. This interaction generates electron-hole pairs primarily through photoelectric effect. An electric field is applied across the a-Se layer, typically 10–15 V per µm thickness of a-Se layer, and approximately 15–20 electron-hole pairs are generated for each interacting 1 keV x-ray photon [40]. The generated charges produce a signal at the readout electrode. Figure 1.13 shows a schematic representation of the detector.

Until recently, amorphous selenium-based direct-conversion detectors utilized flat-panel amorphous silicon thin-film transistor (TFT) arrays for charge readout. Figure 1.14 shows a schematic of such a thin-film transistor readout. Similar to the readout used in amorphous silicon-based indirect-conversion detectors, the presence of bias, gate, and data lines and the thin-film transistor results in a fill factor that is approximately 70%. Currently, a-Se detectors with TFT readout are available either with 70 µm pixels or with 85 µm pixels. One important characteristic that direct-conversion amorphous selenium exhibits is excellent spatial resolution. This high spatial resolution can be observed through their MTF characteristics [41], shown in Figure 1.15 for an a-Se detector with 70 µm pixel pitch. The MTF approaches the theoretical expectation of an ideal pixel response with small degradation due to charge trapping [42]. Measured DQE characteristics [41] using a 28 kVp Mo/Mo spectrum with 2 mm of Al added to the x-ray tube port for an a-Se detector with 70 µm pixel pitch are shown in Figure 1.16. Low-frequency DQE of approximately 60% is observed at exposure levels relevant to mammography. Similar results have also been reported for a system using 85 µm pixel pitch [42].

There has been considerable research interest in developing optical readout technology in an effort to minimize the

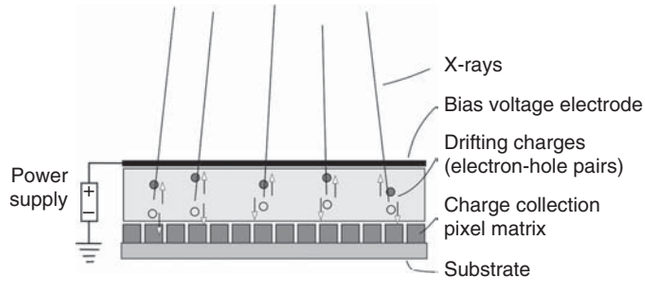

Figure 1.13 Schematic of an amorphous selenium (a-Se)-based direct-conversion detector.

electronic noise that arises from TFT readout [43–46]. Recently, an a-Se-based system that utilizes an additional photoconductive layer with a 50 µm pixel pitch has been developed, and this has shown desirable physical characteristics [46].

Digital cassette mammography

Digital mammography with flat-panel detectors using direct and indirect-conversion methods represents a top-tier technology in terms of radiation dose efficiency, contrast, and spatial resolution. These devices are completely integrated with the x-ray system and cannot be used to upgrade film-screen systems to digital mammography. Therefore, with the rapid conversion from film-screen to digital mammography, even relatively recent film-screen mammography units will have to be discarded if a facility decides to upgrade to digital mammography. The conversion to digital by using a digital cassette is a concept that has been discussed for many years. Photostimulable phosphor plates (also called CR, for computed radiography) incorporated in a portable cassette have been widely used in general radiography for many years and they are now the most widely used digital technology for general radiography. CR-based digital cassette mammography provides a cost-efficient approach for upgrading a facility with multiple film-screen systems to digital mammography, but is yet to demonstrate objective image quality metrics that are similar to dedicated flat-panel detector-based digital mammography systems.

In computed radiography, a photostimulable phosphor plate, also called an image plate (IP), is used as the primary detector of x-rays similar to film-screen mammography or scintillator-based indirect-conversion detectors. This IP is incorporated in a cassette that is identical in dimensions and form to a film-screen mammography cassette, and it is intended to be used in place of a film-screen cassette in mammography units. During mammographic exposure, x-rays transmit past the breast, breast support plate, antiscatter grid, and the digital cassette cover, prior to absorption in the photostimulable phosphor primarily by the photoelectric effect. This generates electron-hole pairs and a fraction of the generated charge is trapped in the crystal structure, creating a latent image proportional to the energy of the

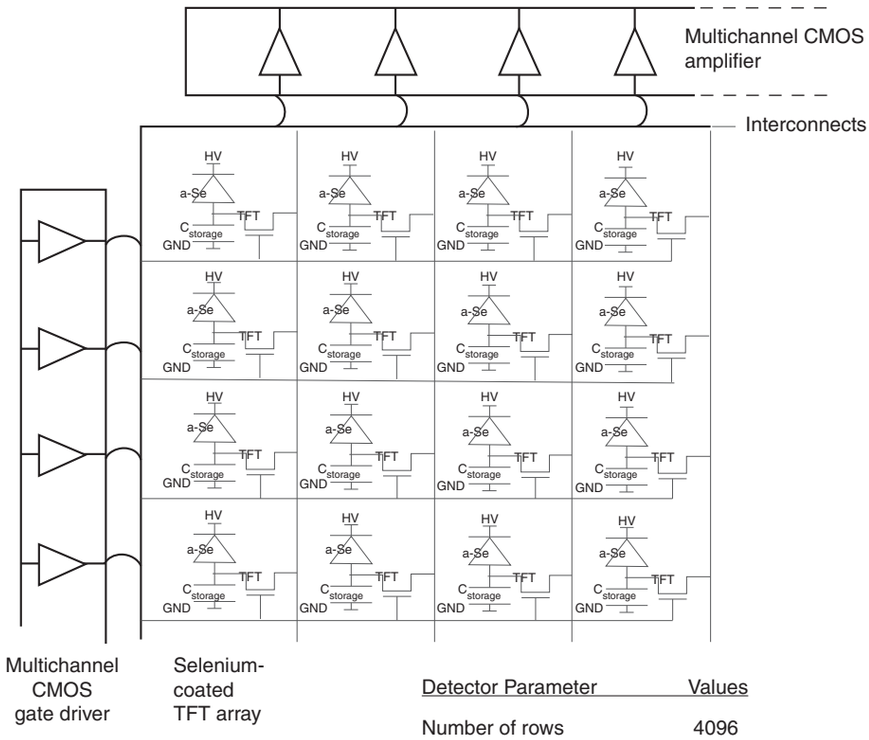

Figure 1.14 Schematic of a thin-film transistor (TFT) array used for charge readout in a-Se detectors. Courtesy of Hologic, Inc., Bedford, MA.

Detector Parameter	Values
Number of rows	4096
Number of columns	3584
Pixel pitch	70 µm
Fill factor	>75%
Quantum absorption efficiency	>95%

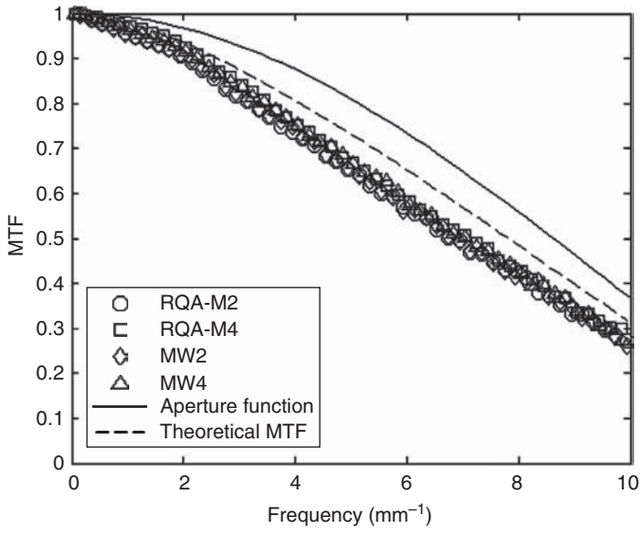

Figure 1.15 MTF characteristics of a prototype a-Se-based digital mammography system with 70 µm pixel pitch. Reproduced with permission from Saunders *et al.*, *Med Phys* 2005; **32**: 588–99 [41]. © American Association of Physicists in Medicine.

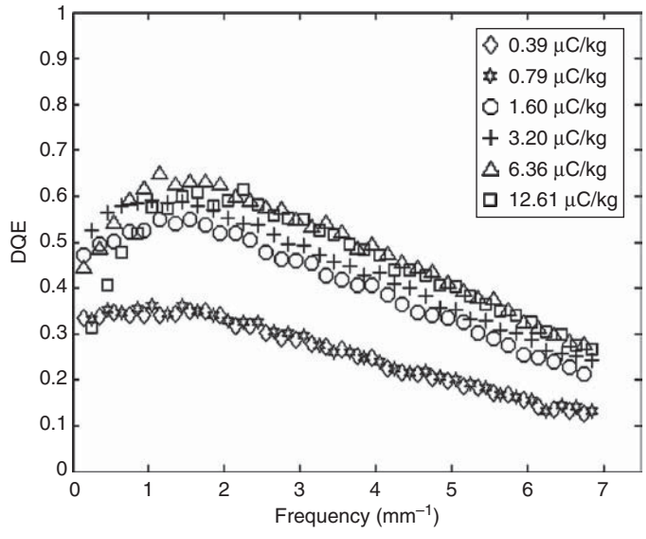

Figure 1.16 DQE characteristics of a prototype amorphous selenium (a-Se)-based digital mammography system with 70 µm pixel pitch. Reproduced with permission from Saunders *et al.*, *Med Phys* 2005; **32**: 588–99 [41]. © American Association of Physicists in Medicine.